

Improved understanding of how irrigated area expansion enhances precipitation recycling by land–atmosphere coupling

Xuanxuan Wang^{a,b,c}, Yongming Cheng^{a,b}, Liu Liu^{a,b,*}, Qiankun Niu^d, Guanhua Huang^{a,b}

^a State Key Laboratory of Efficient Utilization of Agricultural Water Resources, China Agricultural University, Beijing 100083, China

^b Center for Agricultural Water Research in China, China Agricultural University, Beijing 100083, China

^c State Key Laboratory of Simulation and Regulation of Water Cycle in River Basin, China Institute of Water Resources and Hydropower Research, Beijing 100038, China

^d Water and Development Research Group, Aalto University, Espoo 00076, Finland

ARTICLE INFO

Handling Editor - Dr. B.E. Clothier

Keywords:

Irrigation effect
Atmospheric–terrestrial interactions
Evapotranspiration
Moisture transport
Water vapor
Northwest China

ABSTRACT

Large-scale agricultural activities can intensify atmospheric–terrestrial interactions, of which precipitation recycling plays a critical role. During 1982–2018, irrigated area has dramatically expanded in Northwest China (NWC). In this study, a regional precipitation recycling model—the Brubaker model was used to investigate the precipitation recycling ratio (PRR) and recycled precipitation (RP). Evapotranspiration (ET) estimated by the atmospheric–terrestrial water balance method (A–T) was employed to investigate precipitation recycling. Statistically, there was a turning point in 2002 for the rate in irrigated area increase, from 0.07×10^6 ha/year before 2002– 0.217×10^6 ha/year after 2002. There were significant shifts in ET, PRR, and RP in NWC, using the turning point of irrigated area expansion as the line of demarcation. The contribution of the change in irrigated area to PRR increased from 18.3% (1982–2002) to 22.9% (2003–2018) in NWC. Prior to 2002, enhanced RP offset the increased ET by 72.9%. After 2002, the positive effect of irrigated area expansion on precipitation recycling disappeared in NWC. Due to the different climate and irrigation practices at the province level, the variations in irrigated area and their contributions to PRR were examined in three provinces, Xinjiang, Gansu, and Shaanxi. Results based on the Brubaker model and Budyko framework indicate that in Xinjiang and Gansu, the contribution of the irrigated area change after the turning point to PRR were 24.5% and -95.6%, respectively, and there is no potential for continued expansion of irrigated area. In Shaanxi, however, there is potential for continued expansion of irrigated area. The methodology for quantifying the impact of irrigated area change on PRR provides reliable references for the sustainable use of cultivated land and the protection of agricultural water resources.

1. Introduction

Precipitation recycling is a critical aspect of the water cycle (Gao et al., 2020). In precipitation recycling, water evaporates from the land and returns to the local area in the form of rain or snow (Brubaker et al., 1993; Eltahir and Bras., 1996; Gimeno et al., 2012; Van Der Ent et al., 2010). Evapotranspiration (ET) supplies local water vapor for precipitation (Gui et al., 2022a). Another vital source of precipitation is water vapor transported from remote land or remote ocean (Brubaker et al., 1993). Recycled precipitation (RP) and the precipitation recycling ratio (PRR) have been proposed (Ma et al., 2019; Yao et al., 2020) to distinguish precipitation sources and accurately characterize the local

atmospheric–terrestrial water cycle. RP is generated from the water vapor provided by local ET (Dominguez et al., 2006; Li et al., 2020). PRR is the ratio of RP to total precipitation and reflects the intensity of local atmospheric–terrestrial water vapor exchange (Brubaker et al., 1993; Eltahir and Bras., 1996; Holgate et al., 2020; Zhang et al., 2021).

Precipitation recycling has been influenced by diverse factors, including global warming (Algarra et al., 2020), land use change such as afforestation or deforestation (Ellison and Ifejika Speranza, 2020; Hoek van Dijke et al., 2022; Medvigy et al., 2011), and agricultural irrigation (Kemena et al., 2018; Xu and Lin, 2021). Global warming increases the atmospheric water holding capacity (Tabari, 2020), intensifies the exchange between the atmosphere and land, which could accelerate

* Correspondence to: State Key Laboratory of Efficient Utilization of Agricultural Water Resources, Center for Agricultural Water Research in China, China Agricultural University, No.17 Tsinghua East Road, Beijing 100083, China.

E-mail address: liuliu@cau.edu.cn (L. Liu).

<https://doi.org/10.1016/j.agwat.2024.108904>

Received 24 September 2023; Received in revised form 27 May 2024; Accepted 27 May 2024

Available online 31 May 2024

0378-3774/© 2024 The Authors. Published by Elsevier B.V. This is an open access article under the CC BY-NC license (<http://creativecommons.org/licenses/by-nc/4.0/>).

precipitation recycling. Large-scale land use change tends to modify physical properties of land surfaces including vegetation cover, soil moisture, and albedo (Li et al., 2018; te Wierik et al., 2021). These changes inevitably alter water and energy partitioning, which in turn control the processes of atmospheric–terrestrial water vapor interaction and precipitation recycling (Sen Roy et al., 2011). Tree restoration directly promotes *ET* and indirectly promotes precipitation by enhancing atmospheric water vapor recycling (Hoek van Dijke et al., 2022). In the Congo Basin and Southern Asia, a modeling study indicates forest greening enhances precipitation recycling which, in turn, supplies soil moisture or increases runoff (Zeng et al., 2018). By contrast, deforestation inhibits precipitation recycling (Medvigy et al., 2011). As a consequence of atmosphere–vegetation feedback, precipitation has decreased in the Amazon in response to a reduction in atmospheric water vapor provided by *ET* (Spracklen and Garcia-Carreras, 2015).

Agricultural irrigation is the most water-consuming sector and accounts for > 2/3 of all global freshwater withdrawal (Siebert et al., 2010). In addition, large-scale agricultural irrigation has a non-negligible impact on precipitation recycling (Zeng et al., 2022). While consuming large amounts of surface and subsurface water, agricultural irrigation can increase soil moisture (Liu et al., 2021), promote *ET* from irrigated area (Yang et al., 2019), increase local precipitation (Pei et al., 2016), which in turn enhances the precipitation recycling (Harding and Snyder, 2012; Lo and Famiglietti, 2013). In Northern India, Eastern Pakistan, and Northern China, heavy irrigation has led to localized increases in precipitation (Wei et al., 2013). In the Taklamakan Desert, where the local atmospheric conditions have become warmer and wetter, precipitation increased thanks to the expansion of irrigated agriculture, leading to enhanced precipitation recycling (Xu and Lin, 2021). During the post Green Revolution period (1980–2005), precipitation increased by 121% in the growing seasons and soil moisture was elevated in response to the rapid expansion in irrigated agriculture in Northwestern India (Sen Roy et al., 2011). Irrigation in the Central Valley of California facilitated the formation of precipitation through atmospheric water vapor convergence, and summer precipitation increased by 15% in response to strengthened regional precipitation recycling (Lo and Famiglietti, 2013). Irrigation and afforestation of the Sahara in Northern Africa enhanced *ET* and precipitation, and could thereby reduce water for irrigation (Kemena et al., 2018). Hence, desert greening in Sahara had a positive effect (Bowring et al., 2014).

In theory, irrigation and greening could enhance water vapor transport via *ET* from the wetter land to the atmosphere (Pei et al., 2016). However, it is difficult to observe *ET* directly on a large scale (Gao et al., 2012). The traditional terrestrial water balance method has been adopted to estimate *ET* (Ohta et al., 2008; Sun et al., 2018). Nevertheless, it is constrained by the terrestrial water storage timespan and the time lag effects could substantially affect the accuracy of *ET* estimation (Moghim, 2020; Wang et al., 2021). In contrast, the atmospheric–terrestrial water balance method considers horizontal divergence of the vapor flux (∇Q) and changes in column water vapor (W) (Yan et al., 2020). In this manner, it provides a novel way to estimate long-term *ET*. Accurate calculation of *ET* is necessary to characterize precipitation recycling, especially for regions with rapid expansion of irrigated agriculture.

Few studies have explored the effect of irrigated area expansion on *PRR* from the perspective of land–atmosphere coupling (Yu et al., 2016; Zemp et al., 2017; Zeng et al., 2018) and quantified the contribution of irrigated area change to *PRR* (Jódar et al., 2010; Shan et al., 2018). Northwest China (NWC) was selected as the study region as it has undergone remarkable expansion of its irrigated area. *PRR*, *RP*, and *ET* were investigated to clarify the variations in precipitation recycling due to irrigated area expansion. The main objectives of present study were to: (1) investigate the variations in irrigated area, precipitation, and water vapor transported into NWC (Q_{in}); (2) accurately estimate *ET* in NWC by the atmospheric–terrestrial water balance method; (3) identify precipitation recycling and the contribution of irrigated area change to

PRR; and (4) explore the potential for irrigated area expansion in NWC.

2. Materials and methods

2.1. Study area

NWC is highly sensitive to global climate change (Li et al., 2012). It is located in the central part of the Eurasian continent and includes the provinces of Xinjiang, Qinghai, Gansu, Shaanxi, and Ningxia as well as western Inner Mongolia (Fig. 1). Its average annual precipitation is < 300 mm and it is considered a typical arid/semi-arid region (Li et al., 2017; Wang et al., 2017). The major crop types in NWC include wheat, corn, and cotton and agricultural irrigation accounts for > 90% of the total water withdrawal (Shen et al., 2013). Over the past few decades, the irrigated area has significantly expanded in NWC in response to continuous population growth and socioeconomic development. There has been a rapid expansion of irrigation and an increase in water consumption in NWC (Han et al., 2016). In NWC, regions with annual precipitation less than 300 mm account for over 70%, and precipitation has also sharply increased over the past 50 years (Deng et al., 2014; Li et al., 2016). However, this trend has significantly declined since the onset of the 21st century (Chen et al., 2015; Yao et al., 2022). Hence, exploring precipitation recycling in the context of expanding irrigated area is crucial for the management and sustainable development of water resources in NWC and other arid and semi-arid regions.

2.2. Data

2.2.1. Data used to obtain irrigated area

Annual spatial cultivated area (*CA*) data for 1982–2018 were obtained from the National Earth System Science Data Center (NESSDC) and the National Science & Technology Infrastructure of China (<http://www.geodata.cn/data/datadetails.html?dataguid=250075179225195&docid=7768>, accessed on January 25, 2022), with a spatial resolution of 0.1°. The proportion of irrigated area (*IA*) and rainfed area (*RA*) to the total cultivated area was determined according to Land-Use Harmonization (<https://luh.umd.edu/data.shtml>, accessed on October 14, 2022) with a spatial resolution of 0.5° (Hurt et al., 2020) and National Bureau of Statistics of China (<https://data.stats.gov.cn/english/>, accessed on October 14, 2022) at the province level.

2.2.2. Precipitation data

Monthly precipitation data were obtained from the China Meteorological Forcing Dataset (CMFD) provided by the National Tibetan Plateau Data Center (TPDC) (<https://data.tpdc.ac.cn/zh-hans/data/8028b944-daaa-4511-8769-965612652c49/>, accessed on June 12, 2021) (He et al., 2020; Yang et al., 2010), with a spatial resolution of 0.1°. CMFD was made through fusion of in-situ observation data at weather stations, remote sensing products and reanalysis dataset. CMFD was developed specifically for studies of land surface processes in China and provides precipitation information with high temporal and spatial resolution.

2.2.3. Data for *ET* estimation based on atmospheric–terrestrial water balance method

The fifth-generation reanalysis product of the European Centre for Medium-Range Weather Forecasts (ERA5) (<https://cds.climate.copernicus.eu/cdsapp#!/dataset/reanalysis-era5-single-levels-monthly-means?tab=form>, accessed on January 12, 2022) provided monthly precipitation (P , mm), specific humidity (q , kg/kg), eastward component of the wind (u , m/s), northward component of the wind (v , m/s), divergence of the vapor flux (∇Q , mm), and column water vapor (W , mm), with a spatial resolution of 0.1° (Hersbach et al., 2020).

2.2.4. Data for *ET* evaluation

Four monthly *ET* products were used to evaluate *ET* estimated by the

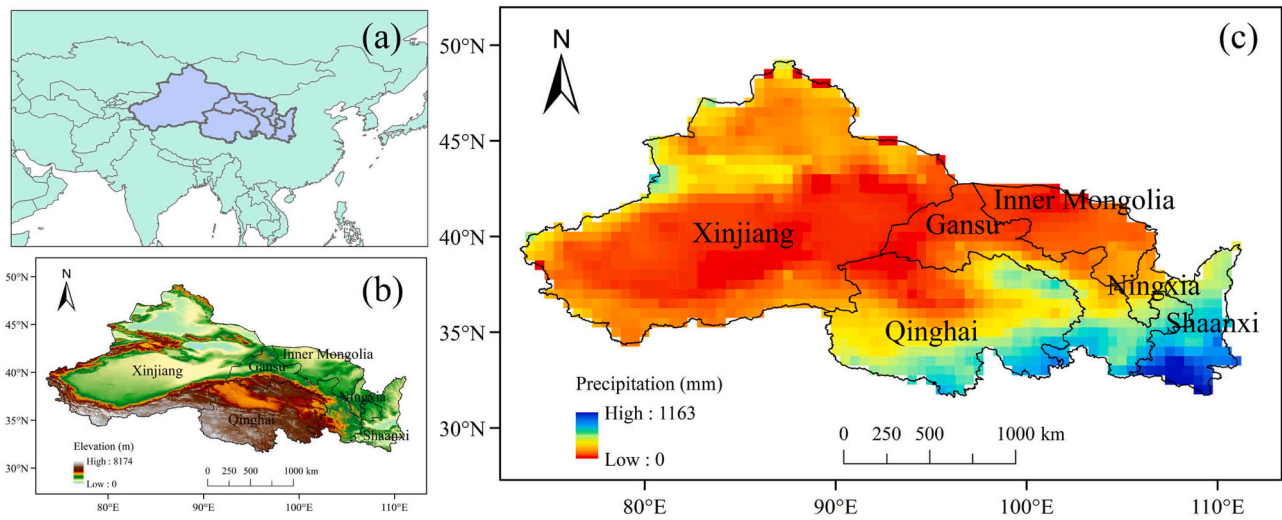


Fig. 1. Location of (a) Northwest China (NWC) from the National Tibetan Plateau Data Center (<http://data.tpdc.ac.cn/>), spatial distribution of elevation (b) and annual precipitation (c).

atmospheric–terrestrial water balance method (A–T) for the period of 2003–2017. Global Land Surface Data Assimilation System (GLDAS) (https://disc.gsfc.nasa.gov/datasets/GLDAS_NOAH025_M_2.1/su [mmmary?keywords=GLDAS](https://disc.gsfc.nasa.gov/datasets/GLDAS_NOAH025_M_2.1/su), accessed on February 20, 2022) (Rodell et al., 2004) and Global Land Evaporation Amsterdam Model (GLEAM v3.5a) (<https://www.gleam.eu/>, accessed on February 25, 2022) (Miralles et al., 2011) provided ET with a spatial resolution of 0.25° . TPDC (Ma and Szilagyi, 2019) and ERA5 provided ET with a spatial resolution of 0.1° .

2.3. Methodology

2.3.1. Data pre-processing

All spatial data were uniformed to a resolution of 0.5° for comparison and analysis. The irrigated area and rainfed area were separated from the cultivated area according to the proportion of irrigated area and rainfed area to the total cultivated area, which was calculated by the following formula:

$$CA = IA + RA \quad (1)$$

$$IA = CA \cdot P_{IA} \quad (2)$$

$$RA = CA \cdot P_{RA} \quad (3)$$

where CA is the cultivated area (ha), IA is the irrigated area (ha), and RA is the rainfed area (ha), P_{IA} is the proportion of irrigated area (%), P_{RA} is the proportion of rainfed area (%). Cultivated area with a spatial resolution of 0.1° could be unified to 0.5° through resampling.

2.3.2. Model description

2.3.2.1. ET estimation based on atmospheric–terrestrial water balance method. The atmospheric–terrestrial water balance method was used to estimate ET . ET estimated by the atmospheric–terrestrial water balance method was based on monthly ERA5 data.

The atmospheric–terrestrial water balance method (Peixoto and Oort, 1983) is applied as follows:

$$ET = P + \nabla Q + \frac{\Delta W}{\Delta t} \quad (4)$$

where ∇Q is the horizontal divergence of the vapor flux (mm/month) and $\frac{\Delta W}{\Delta t}$ is the change in column water vapor (mm/month).

$\frac{\Delta W}{\Delta t}$ is calculated as follows:

$$\frac{\Delta W}{\Delta t} = W_i - W_{i-1} \quad (5)$$

where W_i is the column water vapor in the i^{th} month (mm/month) and W_{i-1} is the column water vapor in the $(i-1)^{\text{th}}$ month (mm/month).

The horizontal vapor flux (Q , $\text{kg m}^{-1}\text{s}^{-1}$) and ∇Q are calculated as follows:

$$Q = \frac{1}{g} \int_{p_s}^{p_T} V \cdot q dp \quad (6)$$

$$\nabla Q = \frac{\partial}{\partial x} \left(\frac{uq}{g} \right) + \frac{\partial}{\partial y} \left(\frac{vq}{g} \right) \quad (7)$$

where g is the gravitational acceleration (9.8 m/s^2), P_T is the top-level atmospheric pressure (hPa), P_S is the pressure at the land surface (hPa), q is the specific humidity (kg/kg), V is the horizontal wind velocity vector (m/s), x is the zonal distance (m), y is the meridional distance (m), u is the zonal component of the wind velocity vector (m/s), and v is the meridional component of the wind velocity vector (m/s).

2.3.2.2. Precipitation recycling model. The PRR and RP were calculated by taking the entire NWC and different provinces as a whole. Based on the Brubaker model, the total precipitation is composed of advective and evaporative sources:

$$P = P_a + P_m \quad (8)$$

where P_a is the fraction of the precipitation from advective water vapor and P_m is the fraction of the precipitation from ET . P_a is from water vapor outside the region and P_m is from local water vapor.

PRR and RP are calculated as follows:

$$PRR = \frac{P_m}{P} \quad (9)$$

$$RP = P_m = P \cdot PRR \quad (10)$$

P_a , P_m , and ET are treated as constants and are represented by their averages (Fig. 2). Thus, there are linear increases in the evaporated and advected water vapor (Brubaker et al., 1993). The horizontal fluxes of the advected water vapor (Q_a) and the evaporated water vapor (Q_m) over the region are calculated as follows:

$$Q_a = \frac{F_{in} + (F_{in} - P_a \cdot A)}{2} = F_{in} - \frac{P_a \cdot A}{2} \quad (11)$$

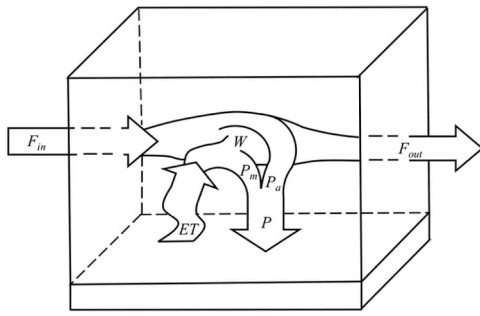


Fig. 2. Conceptual precipitation recycling model based on the Brubaker model. ET is the evapotranspiration, P is the precipitation, F_{in} is the column-integrated water vapor transported into a terrestrial region, F_{out} is the column-integrated water vapor transported out of a terrestrial region, P_a is the fraction of precipitation from advective water vapor, and P_m is the fraction of precipitation from ET , W is the column water vapor.

$$Q_m = \frac{0 + (ET - P_m) \cdot A}{2} = \frac{(ET - P_m) \cdot A}{2} \quad (12)$$

where Q_a is the water vapor transported from outside and Q_m is the water vapor provided by ET .

Assuming a fully mixed atmosphere:

$$\frac{P_a}{P_m} = \frac{Q_a}{Q_m} \quad (13)$$

PRR is calculated as follows:

$$PRR = \frac{ET \cdot A}{ET \cdot A + 2F_{in}} = \frac{ET}{ET + 2Q_{in}} \quad (14)$$

$$Q_{in} = \frac{F_{in}}{A} \quad (15)$$

where F_{in} is the column-integrated water vapor transported into a terrestrial region, A is the area of the terrestrial region, and Q_{in} is the column-integrated water vapor (mm).

2.3.2.3. Attribution of change in PRR . The contribution of the irrigated area (C_{IA}) was proposed to quantify the effects of change in irrigated area (IA) on the change in PRR through ET . A similar approach was used in the Budyko framework (Budyko, 1974; Xu et al., 2014). The derivation method of calculating the contribution of the irrigated area change to the change in PRR (C_{IA}) through Q_{in} and the elasticity coefficient (ϵ_{IA}) was similar to that used for C_{IA} and ϵ_{IA} . Therefore, relevant equations were included in Text S1 of the [Supplementary Material](#).

The partial derivative of PRR for ET is expressed as:

$$\frac{\partial PRR}{\partial ET} = \frac{2Q_{in}}{(ET + 2Q_{in})^2} \quad (16)$$

Before calculating C_{IA} , the elasticity coefficient (ϵ_{IA}) was determined to characterize the sensitivity of IA to PRR (Xin et al., 2021):

$$\epsilon_{IA} = \frac{\partial PRR}{\partial IA} \cdot \frac{IA}{PRR} = \frac{\partial PRR}{\partial ET} \cdot \frac{\partial ET}{\partial IA} \cdot \frac{IA}{PRR} = \frac{2Q_{in}}{(ET + 2Q_{in})^2} \cdot \frac{\partial ET}{\partial IA} \cdot \frac{IA}{PRR} \quad (17)$$

$$\frac{\Delta PRR_{IA}}{PRR} = \epsilon_{IA} \cdot \frac{\Delta IA}{IA} \quad (18)$$

$$C_{IA} = \frac{\Delta PRR_{IA}}{\Delta PRR} = \epsilon_{IA} \cdot \frac{\Delta IA}{IA} \cdot \frac{PRR}{\Delta PRR} \quad (19)$$

$$C_{IA} = \frac{2Q_{in}}{(ET + 2Q_{in})^2} \cdot \frac{\partial ET}{\partial IA} \cdot \frac{IA}{PRR} \cdot \frac{\Delta IA}{IA} \cdot \frac{PRR}{\Delta PRR} = \frac{2Q_{in}}{(ET + 2Q_{in})^2} \cdot \frac{\partial ET}{\partial IA} \cdot \frac{\Delta IA}{\Delta PRR} \quad (20)$$

where ΔIA is the change in IA during a specific period, ΔPRR is the change in PRR during the same time period, and ΔPRR_{IA} is the change in PRR caused by ΔIA .

2.3.3. Evaluation metrics for all results

Four ET products from TPDC, ERA5, GLDAS, and GLEAM were used to systematically evaluate ET estimated by the atmospheric-terrestrial water balance method. Correlation coefficient (R) and root mean square error ($RMSE$) were used to evaluate ET derived from four products and A-T.

$$R = \frac{\sum_{i=1}^n (x_i - \bar{x}) \cdot (y_i - \bar{y})}{\sqrt{\sum_{i=1}^n (x_i - \bar{x})^2} \cdot \sqrt{\sum_{i=1}^n (y_i - \bar{y})^2}} \quad (21)$$

$$RMSE = \sqrt{\frac{\sum_{i=1}^n (x_i - y_i)^2}{n}} \quad (22)$$

where x_i is the variable to be evaluated, y_i is the corresponding baseline variable, the overbar is the average value, and n is the number of data pairs.

2.3.4. Identification of turning point and threshold for irrigated area

The Pettitt test was employed to identify turning point of irrigated area in the NWC and its three provinces during 1982–2018. Relevant equations for the Pettitt test were summarized in Text S2 of the [Supplementary Material](#). Threshold is a value within which irrigated area expansion can enhance precipitation recycling. The simultaneous increase or decrease in irrigated area and PRR indicates that the irrigated area has not exceeded the threshold.

3. Results

3.1. Characteristics of the variations in irrigated area, precipitation, and Q_{in} in NWC

Fig. 3 shows that the irrigated area significantly expanded ($p < 0.01$) at the rate of 0.17×10^6 ha/year between 1982 and 2018. The irrigated area expanded from 2.88×10^6 ha in 1982– 8.23×10^6 ha in 2018 and the rate of increase was 185.8%. During 1982–2018, irrigated area change in Xinjiang accounted for 74.1% of the NWC. The results based on the Pettitt test indicated a change point in 2002 for the rate in irrigated area increase (**Fig. S1**), from 0.07×10^6 ha/year to 0.217×10^6 ha/year. The irrigated area had significantly increased ($p < 0.01$) at the rate of 0.07×10^6 ha/year before 2002. After 2002, the irrigated area had significantly increased ($p < 0.01$) at the rate of 0.217×10^6 ha/year, three times as much as before 2002. Precipitation also significantly increased ($p < 0.01$) between 1982 and 2018 at the rate of 2.47 mm/year. Precipitation in NWC significantly increased ($p < 0.05$) at the rate of 2.16 mm/year before 2002 and slightly decreased thereafter, consistent with previous studies (Peng and Zhou, 2017; Yang et al., 2017). Precipitation also increased from ~ 183.5 mm to ~ 267.3 mm ($> 40\%$) between 1982 and 2018.

Due to the east-west topography, the NWC was mainly influenced by the water vapor flux along the westerly wind belt in the latitudinal direction (Wu et al., 2019). The column-integrated water vapor transported into NWC (Q_{in}) non-significantly decreased at the rate of 1.32 mm/year between 1982 and 2018. During the period of 1982–2018, the trend of Q_{in} is not clear but with large variations. Q_{in} significantly decreased ($p < 0.05$) at the rate of 7.71 mm/year before 2002 and slightly increased at the rate of 1.02 mm/year thereafter.

However, during the period of 1982–2018, the irrigated area significantly expanded and precipitation significantly increased. The formation of precipitation might depend more on the water vapor provided by local ET . Irrigation and greening could also accelerate precipitation recycling (Pei et al., 2016; Yu et al., 2016). The rapid

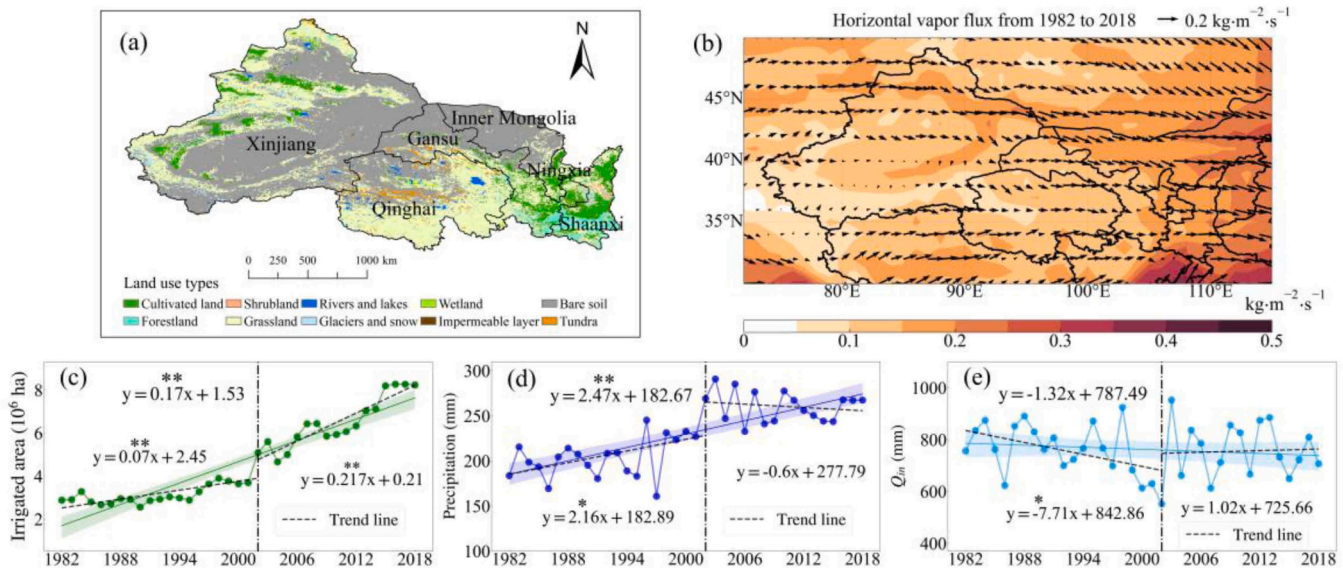


Fig. 3. Land use types (a), horizontal vapor flux (b), irrigated area (c), precipitation (d), and column-integrated water vapor (Q_m) transported into NWC (e). ** represents $p < 0.01$; * represents $p < 0.05$. Vertical dash-dotted line represents dividing year of 2002. Shaded area represents 95% confidence level.

development of irrigated agriculture in NWC may have influenced local precipitation recycling and variations in precipitation. Thus, the mechanisms and the patterns of variation in precipitation recycling must be examined within the context of irrigated area expansion in NWC.

3.2. Accurate ET estimation

3.2.1. Temporal ET verification

The mean, maximum and minimum values of annual ET provided by A-T, ET-TPDC, ET-ERA5, ET-GLDAS, and ET-GLEAM during 2003–2017 are shown in Table 1. Similar to the spatial distribution of precipitation (Fig. 1), ET was relatively higher in southeastern part of the NWC (Fig. S2), especially in Shaanxi and southern Gansu. Temporal and spatial results of ET were provided in the Supplementary Material, including calculations for cool months (September to February) and warm months (March to August) (Fig. S3 and Fig. S4). The ET products from TPDC, ERA5, GLDAS, and GLEAM were used to validate and systematically evaluate ET estimated by the atmospheric-terrestrial water balance method. Fig. 4 shows that all four ET products mutually displayed high R^2 (0.97–0.98) and low RMSE (2.18–11.13 mm/month). Hence, it was reasonable to adopt ET derived from all four products as baselines to evaluate the performance of ET for NWC estimated by the atmospheric-terrestrial water balance method. The scatterplots in Fig. 5 show that ET estimated by atmospheric-terrestrial water balance method was consistent with ET provided by all four products. A-T exhibited considerably high R^2 and low RMSE with respect to ET provided by the four products. When ET-TPDC, ET-ERA5, ET-GLDAS, and ET-GLEAM were the baseline, the R^2 for A-T were 0.93, 0.95, 0.93, and

Table 1

The mean, maximum and minimum values of annual ET.

Annual ET	Average values (mm)	Maximum values (mm)	Minimum values (mm)
A-T	234.6	276.3	209.7
ET-TPDC	247.7	269.2	222.0
ET-ERA5	313.5	332.4	295.9
ET-GLDAS	216.0	233.9	197.1
ET-GLEAM	214.9	243.6	198.5

Note: A-T is ET estimated by atmospheric-terrestrial water balance method. ET-TPDC is ET provided by TPDC. ET-ERA5 is ET provided by ERA5. ET-GLDAS is ET provided by GLDAS. ET-GLEAM is ET provided by GLEAM.

0.94, respectively, while the RMSE for A-T were 5.47 mm/month, 8.58 mm/month, 5.15 mm/month, and 4.79 mm/month, respectively. The scatterplots for irrigated area, rainfed area, grassland and forestland were provided in Supplementary Material (Fig. S5, Fig. S6, Fig. S7 and Fig. S8), including annual, cool months and warm months.

3.2.2. Spatial ET verification

A-T had a high spatial correlation with ET provided by all four products. Fig. 6 shows that the spatial correlation coefficient for A-T reached a maximum of 0.97 and was > 0.5 in most areas when ET-TPDC was the baseline. Similar results were obtained using ET provided by ERA5, GLDAS, and GLEAM as baselines. Fig. 7 shows the spatial distribution of the correlation coefficients between ET provided by the four products and ET estimated by the atmospheric-terrestrial water balance method. Overall, A-T made accurate spatial characterizations of ET in NWC. The spatial correlation coefficients were low only in the central and northern parts of Xinjiang and western Inner Mongolia.

The annual scale correlation results (Fig. S9) also indicated that the atmospheric-terrestrial water balance method could accurately describe the ET in NWC and provided a reliable reference for effective ET estimation. For these reasons, the atmospheric-terrestrial water balance method was used to estimate the long-term (1982–2018) characteristics of the variations in ET and PRR.

3.3. Precipitation recycling and the contribution of change in irrigated area to PRR

ET is the first step in precipitation recycling and the local water vapor source for RP. The variation characteristics of ET in NWC between 1982 and 2018 are shown in Fig. 8. ET was relatively large in areas covered by irrigated land such as Shaanxi, southern Gansu, and western Xinjiang. In contrast, ET was comparatively smaller in desert areas such as the eastern and central parts of Xinjiang, western Inner Mongolia, and northwestern Qinghai and Gansu. There were regions of negative ET and condensed water at the junction of desert and oasis. Sharp nocturnal temperature drops caused water vapor to condense in these areas (Smirnov, 2020). Condensation might also be enhanced by the expansion of irrigated area because ET provided considerable water vapor through water vapor transport. Condensation captured by A-T indicates a land-atmosphere coupling mechanism in NWC. There was a noticeable shift in ET during 1982–2018. ET significantly increased ($p < 0.01$) at the

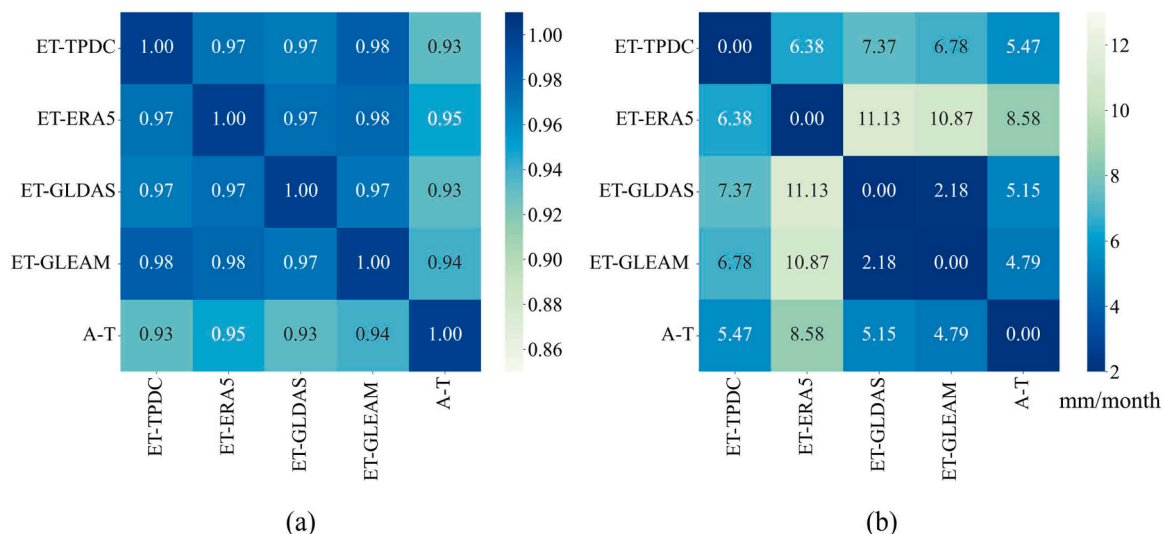


Fig. 4. Heatmap of R^2 (a) and $RMSE$ (b) among monthly ET derived from TPDC, ERA5, GLDAS and GLEAM and by the atmospheric-terrestrial water balance method.

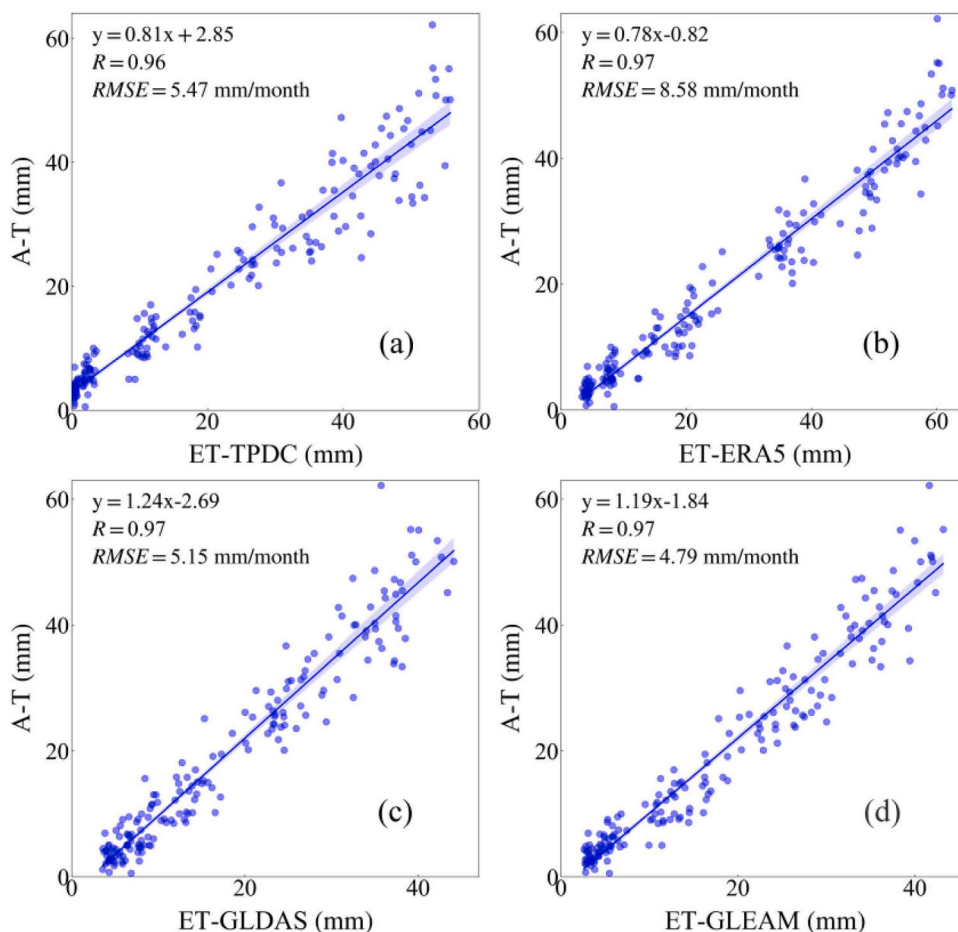


Fig. 5. Scatterplots of monthly ET derived from TPDC (a), ERA5 (b), GLDAS (c), and GLEAM (d) vs. $A-T$. Shaded area represents 95% confidence level.

rate of 1.18 mm/year before 2002 and nonsignificantly decreased at the rate of 1.6 mm/year thereafter. Before 2002, the increase in precipitation and irrigated area contributed to the significant ($p < 0.01$) increase in ET (Kemena et al., 2018). After 2002, although the irrigated area increased, the precipitation decreased nonsignificantly (Deng et al., 2014). In addition, the increased withdrawal of surface water and groundwater for irrigation led to a significant decline in terrestrial water

storage after 2002 (Lai et al., 2022).

PRR in NWC nonsignificantly decreased between 1982 and 2018 at the rate of 0.01%/year. PRR significantly increased ($p < 0.01$) at the rate of 0.21%/year before 2002 and nonsignificantly decreased at the rate of 0.13%/year thereafter. The decrease in PRR after 2002 also caused the decreasing trend in PRR between 1982 and 2018. In addition, PRR increased with the expansion of spatial scale (Fig. S10). RP significantly

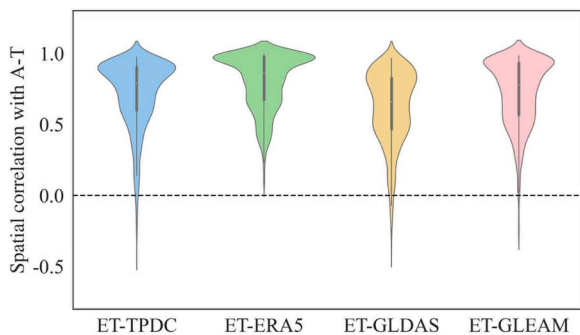


Fig. 6. Violin diagram of spatial correlations between monthly ET provided by four products and A-T.

increased ($p < 0.01$) between 1982 and 2018 at the rate of 0.37 mm/year. *RP* significantly increased ($p < 0.01$) at the rate of 0.86 mm/year before 2002 and reached a maximum of 60.4 mm in 2002 with an increase of ~100%. Before 2002, the elevation in *RP*, precipitation, and *PRR* were consistent with the trend in irrigated area, and the significant increases in precipitation and *PRR* substantially improved *RP*. Moreover, the enhancement of *RP* before 2002 could offset any water loss caused by *ET*. After 2002, *RP* nonsignificantly decreased at the rate of 0.43 mm/year.

The irrigated area is mainly concentrated in Xinjiang, Gansu, and Shaanxi, which account for 59.3%, 16.2%, and 15.5% of the irrigation area in NWC, with a total proportion of more than 90%. Therefore, to further investigate the effects and spatial heterogeneity of irrigated area changes on *PRR*, we examined the variations in irrigated area and their contributions to change in *PRR* in Xinjiang, Gansu, and Shaanxi. Fig. 9 shows that the irrigated area contributed 18.3% to the increase in *PRR* in NWC between 1982 and 2002. Rapid expansion of the irrigated area enhanced precipitation recycling, promoted *RP* and, by extension, significantly increased precipitation. After the turning point (2002), irrigated area in NWC increased more significantly. Consequently, the contribution of irrigated area change to the change in *PRR* increased

from 18.3% to 22.9%, with *PRR* decreased. And the elasticity coefficient changed from positive to negative, indicating that the positive effect of irrigated area expansion on precipitation recycling disappeared after 2002.

Fig. 10 shows that the irrigated area in Xinjiang, Gansu and Shaanxi all increased significantly during the period of 1982–2018. In Xinjiang, both irrigated area and *PRR* significantly increased ($p < 0.01$) before 2000, but *PRR* decreased after 2000. The contribution of the irrigated area to the changes in *PRR* in Xinjiang was 30.7% before 2000 and decreased to 24.5% after 2000. In Gansu, irrigated area significantly increased ($p < 0.05$) as did the *PRR* ($p < 0.01$) before 2002. After 2002, irrigated area significantly increased ($p < 0.01$) whereas the *PRR* nonsignificantly decreased. However, the contribution of the irrigated area to the change in *PRR* decreased from 19.9% to -95.6%. Hence, the positive effect of irrigated area expansion on precipitation recycling in Xinjiang and Gansu disappeared after the turning point, which consumed large amounts of water resources and led to water loss (Harding and Snyder, 2012). In Shaanxi, both irrigated area and *PRR* decreased nonsignificantly before 2006 and increased nonsignificantly after 2006. The contribution of the irrigated area to the change in *PRR* decreased from 121.1% to 14.5%. From the perspective of increasing *PRR*, continued expansion of the irrigated area in Shaanxi is possible, as increased precipitation recycling could mitigate agricultural water consumption (Gui et al., 2022b).

4. Discussion

4.1. Threshold and potential for irrigated area expansion

If the irrigated area and *PRR* increase or decrease simultaneously, it indicates that the irrigated area has not exceeded the threshold. In this case, increased precipitation caused by the expansion of irrigated agriculture could compensate for water loss through *ET* and there is potential for continued expansion. If water loss due to *ET* is much larger than increased precipitation, it indicates that the irrigated area has exceeded the threshold, which results in net water loss (Harding and Snyder, 2012). However, the threshold for irrigated area is related to

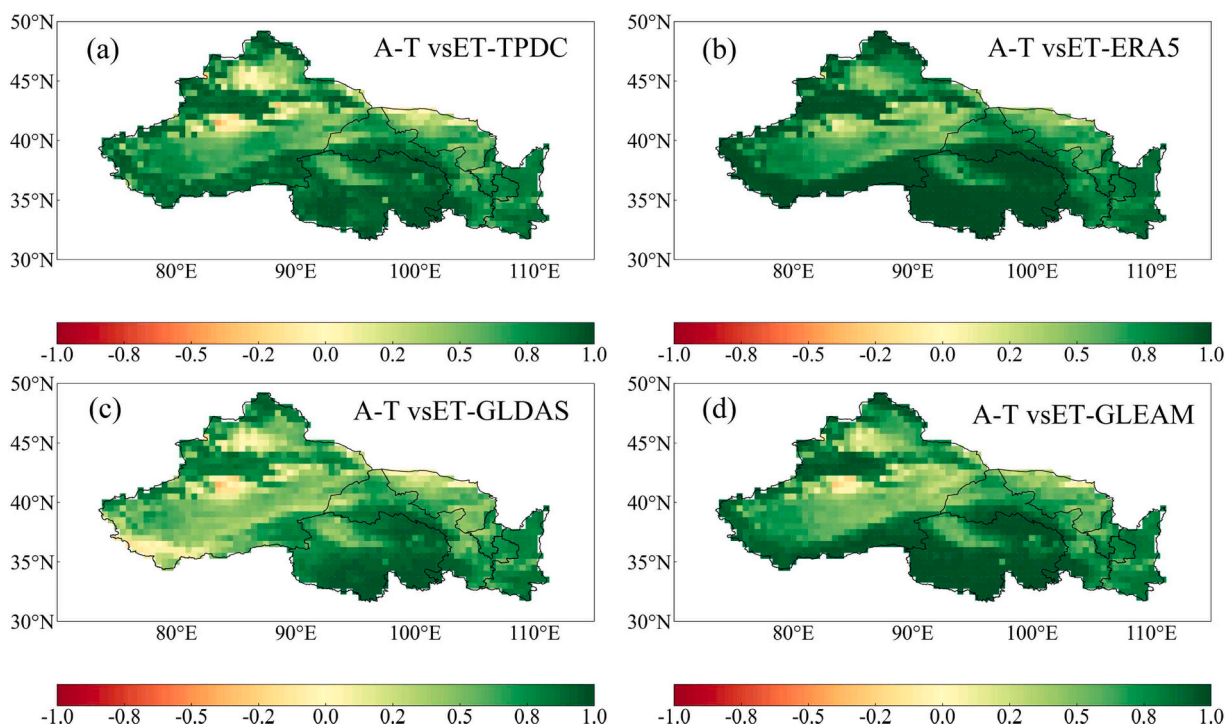


Fig. 7. Spatial distribution of correlation coefficients between A-T and monthly ET provided by TPDC (a), ERA5 (b), GLDAS (c), and GLEAM (d).

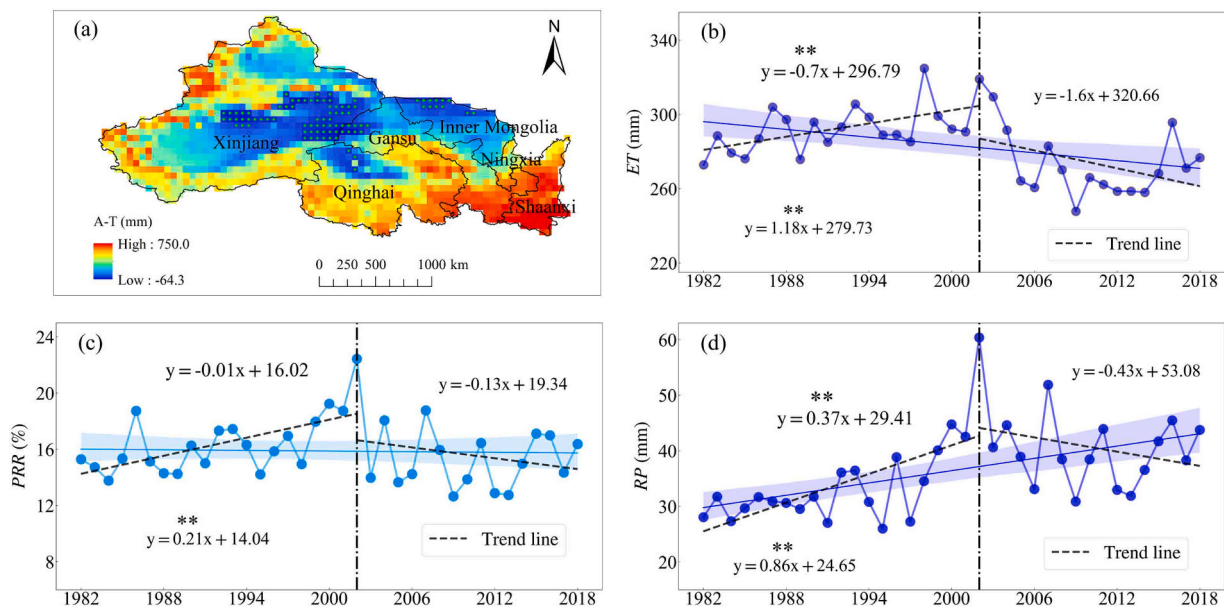


Fig. 8. Spatial distribution of ET (a) and variations in ET (b), PRR (c), and RP (d) in NWC between 1982 and 2018. Green dots represent regions with condensed water. PRR denotes the precipitation recycling ratio and RP denotes the recycled precipitation. Shaded area represents 95% confidence level.

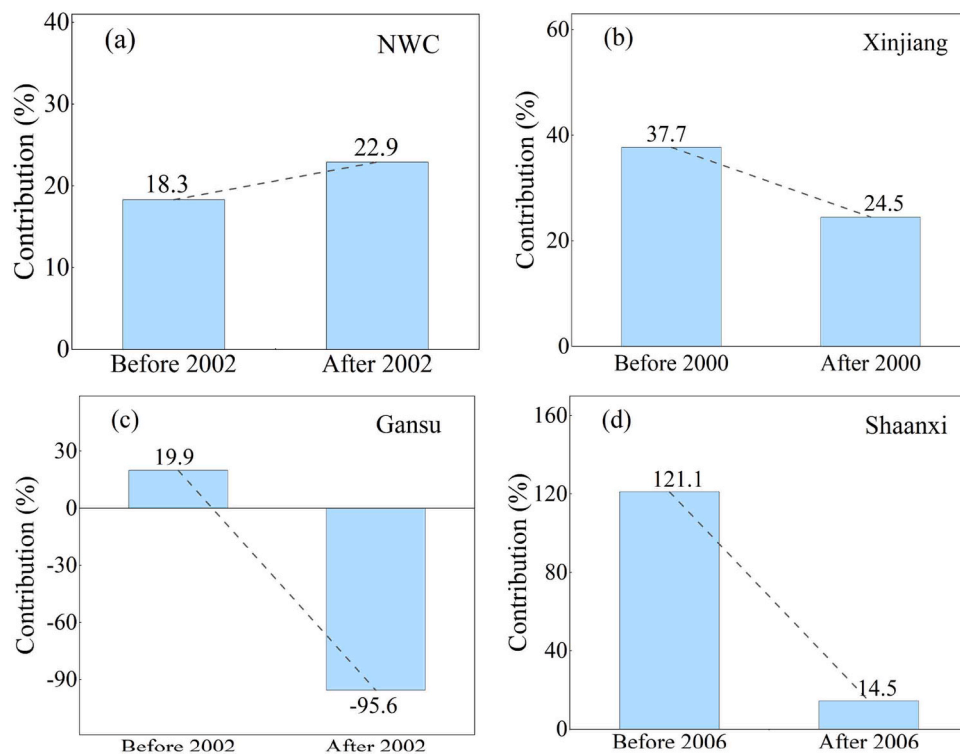


Fig. 9. Contribution of the change in irrigated area to the change in PRR in NWC (a), Xinjiang (b), Gansu (c) and Shaanxi (d) between 1982 and 2018.

precipitation, temperature, irrigation efficiency, atmospheric circulation and other factors (Layton and Ellison, 2016; Pei et al., 2016). The threshold may be relatively high for regions with favorable climatic conditions where water vapor is conducive to precipitation formation (Gui et al., 2022a). Precipitation and terrestrial water storage in Shaanxi are more abundant than those in Gansu and Xinjiang (Lai et al., 2022), so irrigation area in Shaanxi has not exceeded the threshold after the turning point. Recent study has revealed that as irrigation efficiency improved, crop water stress in the Tarim River Basin significantly declined, which in turn raised the threshold for irrigated area (Fu et al.,

2022). Global warming leads to glacier and snow melting and alteration of surface available water resources, which will inevitably affect the stability of threshold and turning point of (Biemans et al., 2019).

Whether expansion of the irrigated area is sustainable deserves concern. In NWC, the contribution of the change in irrigated area to the increase in PRR was 18.3% between 1982 and 2002. Thus, the expansion of irrigated area before 2002 played a non-negligible role in the improvement of PRR. After 2002, the positive effect of irrigated area expansion on precipitation recycling disappeared. The irrigated area in NWC, with a multi-year average of 6.49×10^6 ha after 2002, exceeded

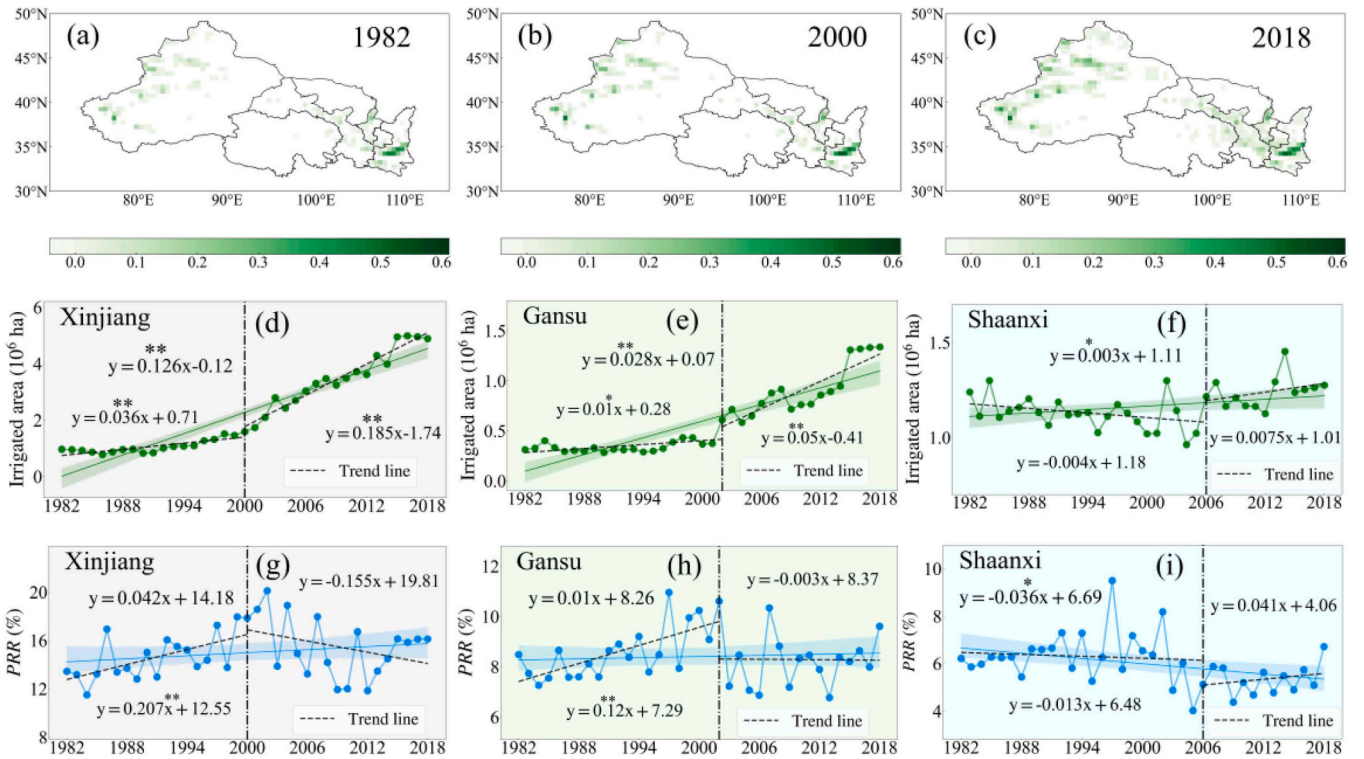


Fig. 10. Spatial distribution and proportion of irrigated area in 1982 (a), 2000 (b) and 2018(c), irrigated area in Xinjiang (d), Gansu (e), and Shaanxi (f), PRR in Xinjiang (g), Gansu (h), and Shaanxi (i). Shaded area represents 95% confidence level.

the threshold and had the opposite effect on PRR. Hence, the threshold of irrigated area in NWC is less than 6.49×10^6 ha.

Xinjiang is the largest province in NWC and the effect of irrigated area expansion on PRR was relatively more apparent there. With the rapid expansion of irrigated area, the PRR showed a decreasing trend after 2000, and the irrigated area in Xinjiang exceeded the threshold. In Gansu, the irrigated area exceeded the threshold, with PRR decreased after the turning point. A study on the Great Plains also indicated that the expansion of irrigated agriculture could result in a net water loss,

because the water loss caused by *ET* was much greater than the increase in *RP* in this region (Harding and Snyder, 2012). Prior to 2006, the reduction of irrigated area in Shaanxi had an inhibitory effect on precipitation recycling. After 2006, expansion of the irrigated area in Shaanxi had a positive effect on the increase in PRR. For this reason, there is potential for continued expansion of the irrigated area in Shaanxi as enhanced precipitation recycling could offset the increase in agricultural water consumption. Similarly, results based on GCM model indicated that increased precipitation caused by irrigation could

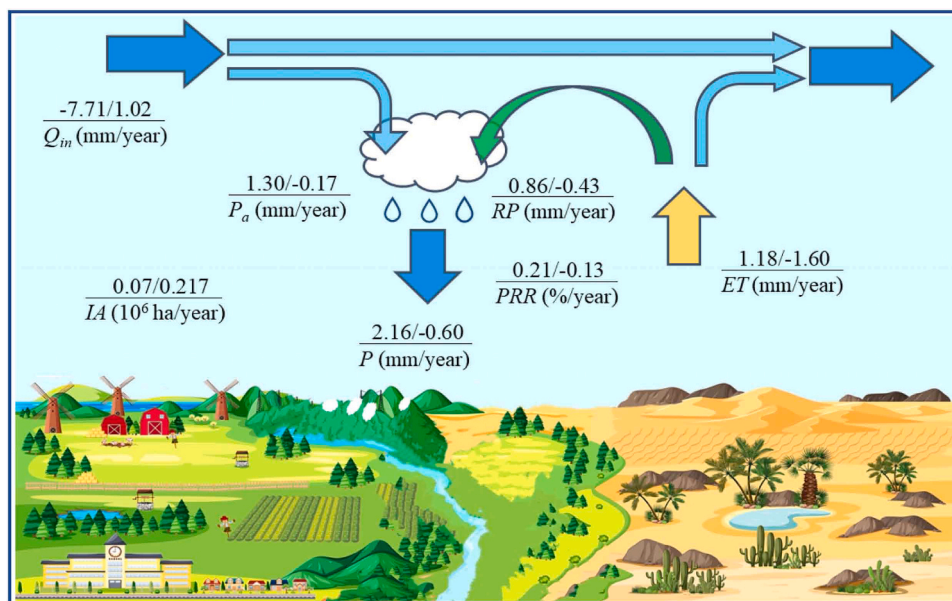


Fig. 11. Precipitation recycling in NWC. 1.18/–1.60 denotes that *ET* increased at the rate of 1.18 mm/year before 2002 and decreased at the rate of 1.60 mm/year after 2002. The same holds true for the other variables. *IA* denotes the irrigated area. Other acronyms remain consistent with those in the previous figure captions.

mitigate the water consumption by *ET* (Ornstein et al., 2009). The positive vegetation–precipitation feedback in the Sahara was dominated by amplified precipitation recycling (Yu et al., 2017).

4.2. Mechanism of change in precipitation recycling

Although *PRR* in NWC did not exceed 25%, the changes in *RP* had a significant impact on the variation in total precipitation. Fig. 11 shows that the rates of increase in total precipitation and *RP* between 1982 and 2002 were 2.16 mm/year and 0.86 mm/year, respectively. In addition, the rates of decrease in total precipitation and *RP* between 2003 and 2018 were 0.60 mm/year and 0.43 mm/year, respectively. The increase in *RP* accounted for 39.8% of the total increase in precipitation before 2002, and the decrease in *RP* accounted for 71.7% of the total increase in precipitation after 2002. Prior to 2002, *ET* increased at the rate of 1.18 mm/year with the irrigated area expanded at the rate of 0.07×10^6 ha/year. The enhancement of *RP* offset the effect of agricultural irrigation on water consumption. In the Southern United States (Wei et al., 2016) and on the Tibetan Plateau (Yan et al., 2020), water vapor is transported from the outside and atmospheric circulation has a strong impact on variations in precipitation. By contrast, NWC is located deep within the central part of the Eurasian continent and is distant from the ocean (Liu et al., 2019). Hence, NWC is more likely to be affected by water vapor originating from local *ET*, compared to the coastal areas. For NWC, *RP* is an essential water source, which can effectively alleviate the contradiction between water supply and demand caused by agricultural expansion (Tuinenburg et al., 2014).

The rapid development of irrigated agriculture in NWC had a non-negligible impact on local precipitation recycling and variations in precipitation. During the period of 1982–2018, the irrigated area significantly expanded and precipitation significantly increased. The formation of precipitation might depend more on the water vapor provided by local *ET*. Thus, it is important to elucidate the mechanisms by which changes in the irrigated area influence precipitation recycling. Irrigation and greening could accelerate precipitation recycling (Pei et al., 2016; Yu et al., 2016). Large-scale expansion in irrigated area alters surface cover and land use, consumes relatively more surface and groundwater resources for agricultural irrigation, enhances *ET*, promotes water vapor exchange between the atmosphere and the land, and increases *RP* and *PRR*. Precipitation in NWC has increased in response to enhanced local precipitation recycling. Moreover, precipitation recycling has seasonality. In summertime, water vapor input from the outside also increases. Nevertheless, *ET* provided by crops in the growing season plays a comparatively more important role in precipitation recycling. During 1982–2018, the annual mean *RP* in the NWC was 65.0 mm, with 53.3 mm in warm months. In NWC, more than 80% of *RP* is concentrated in warm months as the temperature rises, the interaction between the atmosphere and the land is strengthened during the growing season, and precipitation recycling is accelerated, which increases the risk of floods. It has been demonstrated that the risk of floods in Xinjiang is expected to increase due to extreme precipitation, especially in the Tianshan Mountains (Yao et al., 2022). In the arid Heihe River Basin of China, transpiration from vegetation contributes relatively more water vapor to the atmosphere and plays a comparatively greater role in precipitation recycling than soil evaporation (Zhao et al., 2019). *ET* is the primary source of water vapor for growing season precipitation in the agroecosystems of the Canadian Prairies (Raddatz, 2007). Therefore, *ET* could be a vital connection between the change in irrigated area and precipitation recycling.

Climate change intensifies the hydrological cycle (Tabari, 2020). Its remarkable warming effect on NWC and expansion of the irrigated area have accelerated precipitation recycling there. NWC is highly sensitive to global warming. Its temperature has increased by 0.34 °C/decade and has significantly exceeded the global average over the past 50 years (Chen et al., 2015). The increases in temperature have enhanced *ET* and the atmospheric water holding capacity in NWC, triggered more

convective precipitation, and fortified local precipitation recycling (Algarrá et al., 2020). However, with the melting of glacier and snow and the decline in terrestrial water storage (Lai et al., 2022), the sustainability of surface water resources in NWC may be threatened. Therefore, while paying attention to the intensification of precipitation recycling caused by irrigated area expansion, sustaining water cannot be ignored in the context of climate warming.

4.3. Uncertainties and limitations

This study may have some uncertainties and limitations regarding the *PRR* quantification and its calculation model development. The accuracy of *PRR* quantification relies on the methodology for quantifying water vapor transformation attributed to atmospheric–terrestrial interactions. In this study, the Brubaker model used to calculate *PRR* assumed a linear relationship between evaporated and advected water vapor, and set the fraction of the precipitation from advective water vapor and the fraction of the precipitation from *ET* as constants on regional averages. Therefore, Only the *PRR* covering the whole NWC and its three provinces was calculated, but the spatial heterogeneity of *PRR* within the NWC was not investigated. Given that irrigated land is mainly distributed in northwestern Xinjiang, the *PRR* in northwestern Xinjiang may be larger than that in southeastern Xinjiang (Yao et al., 2022). In addition, the contribution of local water vapor provided by *ET* to precipitation in NWC was quantified through *PRR*. It has been demonstrated that the sources of water vapor for precipitation in NWC include the Arctic Ocean, the North Atlantic, the tropical Indian Ocean, and South China Sea (Wu et al., 2019; Yao et al., 2020). During 1982–2018, contribution of the change in irrigated area to the change in *PRR* through Q_{in} was quantified (Fig. S11). However, the contribution of external water vapor from different regions to precipitation in NWC was not explored. These could be clarified in the future by combining other models such as WAM2-layers, FLEXPART etc (Huang and Cui, 2015; Zhang et al., 2017).

The data employed in the study may also give rise to some uncertainties and limitations for our results. In NWC, the radiation is strong and cannot be ignored (Huang et al., 2016). However, the sublimation module in GLEAM does not consider radiation (Li et al., 2019), which may affect the accurate estimation of *ET*–GLEAM and result in uncertainty in the verification of *ET*. In addition, *ET*–TPDC is derived from the complementary–relationship method, with input data including surface temperature and humidity provided by ERA5 (Ma and Szilagyi, 2019). Therefore, *ET*–TPDC and *ET*–ERA5 are not completely independent, which may have an impact the validation of *ET* in NWC.

5. Conclusions

The present study explored the variations in the characteristics of the irrigated area, precipitation, and Q_{in} in NWC between 1982 and 2018. The atmospheric–terrestrial water balance method was used to estimate *ET* and precipitation recycling was investigated based on the Brubaker model and A–T. The contributions of the changes in the irrigated area to *PRR* were quantified for NWC and Xinjiang, Gansu, and Shaanxi Provinces. Moreover, the potential for irrigated area expansion was explored. The main conclusions are summarized as follows.

The atmospheric–terrestrial water balance method could accurately describe the spatiotemporal characteristics of *ET* in NWC and has been verified for different land use types and different time scales. A–T considers atmospheric–terrestrial interactions and external water vapor transport, which lays a solid foundation for the accurate calculation of *PRR* and *RP* in NWC. Expansion of the irrigated area increased the amount of local water vapor that *ET* delivers to the atmosphere which, by extension, enhanced local precipitation recycling. Rapid increases in temperature promote *ET* and atmospheric water holding capacity, had a positive impact on precipitation recycling. However, after 2002, more surface water and groundwater were needed to maintain the rapid

expansion of irrigated area in NWC. In NWC, rapid expansion of the irrigated area enhanced precipitation recycling before 2002, and the irrigated area exceeded the threshold after 2002. In Shaanxi, there is potential for continued expansion of the irrigated area. However, the irrigated area in Xinjiang and Gansu exceeded the threshold after the turning point and needs to be limited.

CRedit authorship contribution statement

Guanhua Huang: Writing – review & editing, Supervision. **Qiankun Niu:** Writing – review & editing, Data curation. **Liu Liu:** Writing – review & editing, Writing – original draft, Validation, Project administration, Methodology, Investigation, Funding acquisition, Formal analysis, Conceptualization. **Yongming Cheng:** Writing – review & editing, Visualization, Methodology, Data curation. **Xuanxuan Wang:** Writing – review & editing, Writing – original draft, Visualization, Validation, Methodology, Formal analysis, Conceptualization.

Declaration of Competing Interest

The authors declare that they have no known competing financial interests or personal relationships that could have appeared to influence the work reported in this paper.

Data availability

Data will be made available on request.

Acknowledgements

This work was jointly supported by the National Natural Science Foundation of China (Grant No. 52379054 and 52079138) and the 2115 Talent Development Program of China Agricultural University (Grant No. 00109019).

Appendix A. Supporting information

Supplementary data associated with this article can be found in the online version at doi:10.1016/j.agwat.2024.108904.

References

- Algarra, I., Nieto, R., Ramos, A.M., Eiras-Barca, J., Trigo, R.M., Gimeno, L., 2020. Significant increase of global anomalous moisture uptake feeding landfalling Atmospheric Rivers. *Nat. Commun.* 11, 1–7. <https://doi.org/10.1038/s41467-020-18876-w>.
- Biemans, H., Siderius, C., Lutz, A.F., Nepal, S., Ahmad, B., Hassan, T., von Bloh, W., Wijnjaard, R.R., Wester, P., Shrestha, A.B., Immerzeel, W.W., 2019. Importance of snow and glacier meltwater for agriculture on the Indo-Gangetic Plain. *Nat. Sustain.* 2, 594–601. <https://doi.org/10.1038/s41893-019-0305-3>.
- Bowring, S.P.K., Miller, L.M., Ganzeveld, L., Kleidon, A., 2014. Applying the concept of “energy return on investment” to desert greening of the Sahara/Sahel using a global climate model. *Earth Syst. Dyn.* 5, 43–53. <https://doi.org/10.5194/esd-5-43-2014>.
- Brubaker, K.L., Entehabi, D., Eagleson, P.S., 1993. Estimation of continental precipitation recycling. *J. Clim.* 6, 1077–1089.
- Budyko, M.I., 1974. *Climte and life*. Academic Press, New York.
- Chen, Y., Li, Z., Fan, Y., Wang, H., Deng, H., 2015. Progress and prospects of climate change impacts on hydrology in the arid region of northwest China. *Environ. Res.* 139, 11–19. <https://doi.org/10.1016/j.envres.2014.12.029>.
- Deng, H., Chen, Y., Shi, X., Li, W., Wang, H., Zhang, S., Fang, G., 2014. Dynamics of temperature and precipitation extremes and their spatial variation in the arid region of northwest China. *Atmos. Res.* 138, 346–355. <https://doi.org/10.1016/j.atmosres.2013.12.001>.
- Dominguez, F., Kumar, P., Liang, X.Z., Ting, M., 2006. Impact of atmospheric moisture storage on precipitation recycling. *J. Clim.* 19, 1513–1530. <https://doi.org/10.1175/JCLI3691.1>.
- Ellison, D., Ifejika Speranza, C., 2020. From blue to green water and back again: promoting tree, shrub and forest-based landscape resilience in the Sahel. *Sci. Total Environ.* 739, 140002 <https://doi.org/10.1016/j.scitotenv.2020.140002>.
- Eltahir, E.A.B., Bras, R.L., 1996. Precipitation recycling. *Rev. Geophys.* 34, 367–378.
- Fu, J., Wang, W., Zaitchik, B., Nie, W., Fei, E.X., Miller, S.M., Harman, C.J., 2022. Critical Role of Irrigation Efficiency for Cropland Expansion in Western China Arid Agroecosystems. *Earth'S. Futur* 10, 1–13. <https://doi.org/10.1029/2022EF002955>.
- Gao, Y., Chen, F., Miguez-Macho, G., Li, X., 2020. Understanding precipitation recycling over the Tibetan Plateau using tracer analysis with WRF. *Clim. Dyn.* 55, 2921–2937. <https://doi.org/10.1007/s00382-020-05426-9>.
- Gao, G., Xu, C.Y., Chen, D., Singh, V.P., 2012. Spatial and temporal characteristics of actual evapotranspiration over Haihe River basin in China. *Stoch. Environ. Res. Risk Assess.* 26, 655–669. <https://doi.org/10.1007/s00477-011-0525-1>.
- Gimeno, L., Stohl, A., Trigo, R.M., Dominguez, F., Yoshimura, K., Yu, L., Drumond, A., Durn-Quesada, A.M., Nieto, R., 2012. Oceanic and terrestrial sources of continental precipitation. *Rev. Geophys.* 50, 1–41. <https://doi.org/10.1029/2012RG000389>.
- Gui, J., Li, Z., Feng, Q., Zhang, B., Xue, J., Gao, W., Li, Y., Liang, P., Nan, F., 2022a. Water resources significance of moisture recycling in the transition zone between Tibetan Plateau and arid region by stable isotope tracing. *J. Hydrol.* 605, 127350 <https://doi.org/10.1016/j.jhydrol.2021.127350>.
- Gui, Y., Wang, Q., Zhao, Y., Ma, M., Li, H., Zhai, J., Li, E., 2022b. On the increased precipitation recycling by large-scale irrigation over the Haihe Plain. *J. Meteorol. Res.* 36, 450–461. <https://doi.org/10.1007/s13351-022-1220-5>.
- Han, S., Tang, Q., Zhang, X., Xu, D., Kou, L., 2016. Surface wind observations affected by agricultural development over Northwest China. *Environ. Res. Lett.* 11 <https://doi.org/10.1088/1748-9326/11/5/054014>.
- Harding, K.J., Snyder, P.K., 2012. Modeling the atmospheric response to irrigation in the great plains. Part II: the precipitation of irrigated water and changes in precipitation recycling. *J. Hydrometeorol.* 13, 1687–1703. <https://doi.org/10.1175/JHM-D-11-099.1>.
- He, J., Yang, K., Tang, W., Lu, H., Qin, J., Chen, Y., Li, X., 2020. The first high-resolution meteorological forcing dataset for land process studies over China. *Sci. Data* 7, 1–11. <https://doi.org/10.1038/s41597-020-0369-y>.
- Hersbach, H., Bell, B., Berrisford, P., Hirahara, S., Horányi, A., Muñoz-Sabater, J., Nicolas, J., Peubey, C., Radu, R., Schepers, D., Simmons, A., Soci, C., Abdalla, S., Abellan, X., Balsamo, G., Bechtold, P., Biavati, G., Bidlot, J., Bonavita, M., De Chiara, G., Dahlgren, P., Dee, D., Diamantakis, M., Dragani, R., Flemming, J., Forbes, R., Fuentes, M., Geer, A., Haimberger, L., Healy, S., Hogan, R.J., Hólm, E., Janisková, M., Keeley, S., Laloyaux, P., Lopez, P., Lupu, C., Radnoti, G., de Rosnay, P., Rozum, I., Vamborg, F., Villaume, S., Thépaut, J.N., 2020. The ERA5 global reanalysis. *Q. J. R. Meteorol. Soc.* 146, 1999–2049. <https://doi.org/10.1002/qj.3803>.
- Hoek van Dijke, A.J., Herold, M., Mallick, K., Benedict, I., Machwitz, M., Schlerf, M., Pranindita, A., Theeuwens, J.J.E., Bastin, J.-F., Teuling, A.J., 2022. Shifts in regional water availability due to global tree restoration. *Nat. Geosci.* 15, 363–368. <https://doi.org/10.1038/s41561-022-00935-0>.
- Holgate, C.M., Evans, J.P., Dijk, I.J.M.V., Pitman, J., Virgilio, G.D.I., 2020. Australian precipitation recycling and evaporative source regions. *J. Clim.* 33, 8721–8735. <https://doi.org/10.1175/JCLI-D-19-0926.1>.
- Huang, Y., Cui, X., 2015. Moisture sources of torrential rainfall events in the sichuan basin of China during summers of 2009–13. *J. Hydrometeorol.* 16, 1906–1917. <https://doi.org/10.1175/JHM-D-14-0220.1>.
- Huang, G., Li, X., Ma, M., Li, H., Huang, C., 2016. High resolution surface radiation products for studies of regional energy, hydrologic and ecological processes over Heihe river basin, northwest China. *Agric. Meteorol.* 230–231, 67–78. <https://doi.org/10.1016/j.agrformet.2016.04.007>.
- Hurttt, G.C., Chini, L., Sahajpal, R., Frolking, S., Bodirsky, B.L., Calvin, K., Doelman, J.C., Fisk, J., Fujimori, S., Goldewijk, K.K., Hasegawa, T., Havlik, P., Heinimann, A., Humpenöder, F., Jungclauss, J., Kaplan, J.O., Kennedy, J., Krisztin, T., Lawrence, D., Lawrence, P., Ma, L., Mertz, O., Pongratz, J., Popp, A., Poulter, B., Riahi, K., Shevliakova, E., Stehfest, E., Thornton, P., Tubiello, F.N., van Vuuren, D.P., Zhang, X., 2020. Harmonization of global land use change and management for the period 850–2100 (LUH2) for CMIP6. *Geosci. Model Dev.* <https://doi.org/10.5194/gmd-13-5425-2020>.
- Jódar, J., Carrera, J., Cruz, A., 2010. Irrigation enhances precipitation at the mountains downwind. *Hydrol. Earth Syst. Sci.* 14, 2003–2010. <https://doi.org/10.5194/hess-14-2003-2010>.
- Kemena, T.P., Matthes, K., Martin, T., Wahl, S., Oschlies, A., 2018. Atmospheric feedbacks in North Africa from an irrigated, afforested Sahara. *Clim. Dyn.* 50, 4561–4581. <https://doi.org/10.1007/s00382-017-3890-8>.
- Lai, J., Li, Y., Chen, J., Niu, G.Y., Lin, P., Li, Q., Wang, L., Han, J., Luo, Z., Sun, Y., 2022. Massive crop expansion threatens agriculture and water sustainability in northwestern China. *Environ. Res. Lett.* 17 <https://doi.org/10.1088/1748-9326/ac46e8>.
- Layton, K., Ellison, D., 2016. Induced precipitation recycling (IPR): a proposed concept for increasing precipitation through natural vegetation feedback mechanisms. *Ecol. Eng.* 91, 553–565. <https://doi.org/10.1016/j.ecoleng.2016.02.031>.
- Li, B., Chen, Y., Shi, X., 2012. Why does the temperature rise faster in the arid region of northwest China? *J. Geophys. Res. Atmos.* 117, 1–7. <https://doi.org/10.1029/2012JD017953>.
- Li, B., Chen, Y., Chen, Z., Xiong, H., Lian, L., 2016. Why does precipitation in northwest China show a significant increasing trend from 1960 to 2010? *Atmos. Res.* 167, 275–284. <https://doi.org/10.1016/j.atmosres.2015.08.017>.
- Li, Z., Chen, Y., Fang, G., Li, Y., 2017. Multivariate assessment and attribution of droughts in Central Asia. *Sci. Rep.* 7, 1–12. <https://doi.org/10.1038/s41598-017-01473-1>.
- Li, X., Long, D., Han, Z., Scanlon, B.R., Sun, Z., Han, P., Hou, A., 2019. Evapotranspiration Estimation for Tibetan Plateau Headwaters Using Conjoint Terrestrial and Atmospheric Water Balances and Multisource Remote Sensing. *Water Resour. Res.* 55, 8608–8630. <https://doi.org/10.1029/2019WR025196>.
- Li, X., Lu, A., Feng, Q., Li, Z., Liu, W., Wang, S., Tripathee, L., Wang, X., Cao, J., 2020. Recycled moisture in an enclosed basin, Guanzhong Basin of Northern China, in the

- summer: contribution to precipitation based on a stable isotope approach. *Environ. Sci. Pollut. Res.* 27, 27926–27936. <https://doi.org/10.1007/s11356-020-09099-z>.
- Li, Y., Piao, S., Li, L.Z.X., Chen, A., Wang, X., Ciais, P., Huang, L., Lian, X., Peng, S., Zeng, Z., Wang, K., Zhou, L., 2018. Divergent hydrological response to large-scale afforestation and vegetation greening in China. *Sci. Adv.* 4, 1–10. <https://doi.org/10.1126/sciadv.aar4182>.
- Liu, H., Chen, Y., Ye, Z., Li, Y., Zhang, Q., 2019. Recent lake area changes in Central Asia. *Sci. Rep.* 9, 1–12. <https://doi.org/10.1038/s41598-019-52396-y>.
- Liu, J., Jin, J., Niu, G.Y., 2021. Effects of Irrigation on Seasonal and Annual Temperature and Precipitation over China Simulated by the WRF Model. *J. Geophys. Res. Atmos.* 126, 1–16. <https://doi.org/10.1029/2020JD034222>.
- Lo, M.H., Famiglietti, J.S., 2013. Irrigation in California's Central Valley strengthens the southwestern U.S. water cycle. *Geophys. Res. Lett.* 40, 301–306. <https://doi.org/10.1002/grl.50108>.
- Ma, N., Szilagyi, J., 2019. The CR of Evaporation: a calibration-free diagnostic and benchmarking tool for large-scale terrestrial evapotranspiration modeling. *Water Resour. Res.* 55, 7246–7274. <https://doi.org/10.1029/2019WR024867>.
- Ma, Q., Zhang, M., Wang, L., Che, Y., 2019. Quantification of moisture recycling in the river basins of China and its controlling factors. *Environ. Earth Sci.* 78 <https://doi.org/10.1007/s12665-019-8404-z>.
- Medvigy, D., Walko, R.L., Avissar, R., 2011. Effects of deforestation on spatiotemporal distributions of precipitation in South America. *J. Clim.* 24, 2147–2163. <https://doi.org/10.1175/2010JCLI3882.1>.
- Miralles, D.G., Holmes, T.R.H., De Jeu, R.A.M., Gash, J.H., Meesters, A.G.C.A., Dolman, A.J., 2011. Global land-surface evaporation estimated from satellite-based observations. *Hydrol. Earth Syst. Sci.* 15, 453–469. <https://doi.org/10.5194/hess-15-453-2011>.
- Moghim, S., 2020. Assessment of Water Storage Changes Using GRACE and GLDAS. *Water Resour. Manag.* 34, 685–697. <https://doi.org/10.1007/s11269-019-02468-5>.
- Ohta, T., Maximov, T.C., Dolman, A.J., Nakai, T., van der Molen, M.K., Kononov, A.V., Maximov, A.P., Hiyama, T., Iijima, Y., Moors, E.J., Tanaka, H., Toba, T., Yabuki, H., 2008. Interannual variation of water balance and summer evapotranspiration in an eastern Siberian larch forest over a 7-year period (1998–2006). *Agric. Meteorol.* 148, 1941–1953. <https://doi.org/10.1016/j.agrformet.2008.04.012>.
- Ornstein, L., Aleinov, I., Rind, D., 2009. Irrigated afforestation of the Sahara and Australian Outback to end global warming. *Clim. Change* 97, 409–437. <https://doi.org/10.1007/s10584-009-9626-y>.
- Pei, L., Moore, N., Zhong, S., Kendall, A.D., Gao, Z., Hyndman, D.W., 2016. Effects of irrigation on summer precipitation over the United States. *J. Clim.* 29, 3541–3558. <https://doi.org/10.1175/JCLI-D-15-0337.1>.
- Peixoto, J.P., Oort, A.H., 1983. The atmospheric branch of the hydrological cycle and climate. *Var. Glob. Water Budg.* 5–65.
- Peng, D., Zhou, T., 2017. Why was the arid and semiarid northwest China getting wetter in the recent decades? *J. Geophys. Res. Atmos.* 122, 9060–9075. <https://doi.org/10.1002/2016JD026424>.
- Raddatz, R.L., 2007. Evidence for the influence of agriculture on weather and climate through the transformation and management of vegetation: illustrated by examples from the Canadian Prairies. *Agric. Meteorol.* 142, 186–202. <https://doi.org/10.1016/j.agrformet.2006.08.022>.
- Rodell, M., Houser, P.R., Jambor, U., Gottschalk, J., Mitchell, K., Meng, C.J., Arsenault, K., Cosgrove, B., Radakovich, J., Bosilovich, M., Entin, J.K., Walker, J.P., Lohmann, D., Toll, D., 2004. The global land data assimilation system. *Bull. Am. Meteorol. Soc.* 85, 381–394. <https://doi.org/10.1175/BAMS-85-3-381>.
- Sen Roy, S., Mahmood, R., Quintanar, A.I., Gonzalez, A., 2011. Impacts of irrigation on dry season precipitation in India. *Theor. Appl. Climatol.* 104, 193–207. <https://doi.org/10.1007/s00704-010-0338-z>.
- Shan, N., Shi, Z., Yang, X., Guo, H., Zhang, X., Zhang, Z., 2018. Oasis irrigation-induced hydro-climatic effects: a case study in the hyper-arid region of Northwest China. *Atmosphere (Basel)* 9. <https://doi.org/10.3390/atmos9040142>.
- Shen, Y., Li, S., Chen, Y., Qi, Y., Zhang, S., 2013. Estimation of regional irrigation water requirement and water supply risk in the arid region of Northwestern China 1989–2010. *Agric. Water Manag.* 128, 55–64. <https://doi.org/10.1016/j.agwat.2013.06.014>.
- Siebert, S., Burke, J., Faures, J.M., Frenken, K., Hoogeveen, J., Döll, P., Portmann, F.T., 2010. Groundwater use for irrigation - a global inventory. *Hydrol. Earth Syst. Sci.* 14, 1863–1880. <https://doi.org/10.5194/hess-14-1863-2010>.
- Smirnov, B.M., 2020. Atmospheric processes involving condensed water. *Phys. Solid State* 62, 24–29. <https://doi.org/10.1134/S106378342001031X>.
- Spracklen, D.V., García-Carreras, L., 2015. The impact of Amazonian deforestation on Amazon basin rainfall. *Geophys. Res. Lett.* 42, 9546–9552. <https://doi.org/10.1002/2015GL066063>.
- Sun, M., Dong, Q., Jiao, M., Zhao, X., Gao, X., Wu, P., Wang, A., 2018. Estimation of actual evapotranspiration in a semiarid region based on grace gravity satellite data-A case study in loess Plateau. *Remote Sens* 10. <https://doi.org/10.3390/rs10122032>.
- Tabari, H., 2020. Climate change impact on flood and extreme precipitation increases with water availability. *Sci. Rep.* 10, 1–10. <https://doi.org/10.1038/s41598-020-70816-2>.
- Tuinenburg, O.A., Hutjes, R.W.A., Stacke, T., Wiltshire, A., Lucas-Picher, P., 2014. Effects of irrigation in India on the atmospheric water budget. *J. Hydrometeorol.* 15, 1028–1050. <https://doi.org/10.1175/JHM-D-13-078.1>.
- Van Der Ent, R.J., Savenije, H.H.G., Schaeffli, B., Steele-Dunne, S.C., 2010. Origin and fate of atmospheric moisture over continents. *Water Resour. Res.* 46, 1–12. <https://doi.org/10.1029/2010WR009127>.
- Wang, X., Liu, L., Niu, Q., Li, H., Xu, Z., 2021. Multiple data products reveal long-term variation characteristics of terrestrial water storage and its dominant factors in data-scarce Alpine Regions. *Remote Sens* 13, 2356. <https://doi.org/10.3390/rs13122356>.
- Wang, H., Pan, Y., Chen, Y., Ye, Z., 2017. Linear trend and abrupt changes of climate indices in the arid region of northwestern China. *Atmos. Res.* 196, 108–118. <https://doi.org/10.1016/j.atmosres.2017.06.008>.
- Wei, J., Dirmeyer, P.A., Wissler, D., Bosilovich, M.G., Mocko, D.M., 2013. Where does the irrigation water go? An estimate of the contribution of irrigation to precipitation using MERRA. *J. Hydrometeorol.* 14, 275–289. <https://doi.org/10.1175/JHM-D-12-079.1>.
- Wei, J., Su, H., Yang, Z.L., 2016. Impact of moisture flux convergence and soil moisture on precipitation: a case study for the southern United States with implications for the globe. *Clim. Dyn.* 46, 467–481. <https://doi.org/10.1007/s00382-015-2593-2>.
- te Wierik, S.A., Cammeraat, E.L.H., Gupta, J., Artzy-Randrup, Y.A., 2021. Reviewing the impact of land use and land-use change on moisture recycling and precipitation patterns. *Water Resour. Res.* 57 <https://doi.org/10.1029/2020WR029234>.
- Wu, P., Ding, Y., Liu, Y., Li, X., 2019. The characteristics of moisture recycling and its impact on regional precipitation against the background of climate warming over Northwest China. *Int. J. Climatol.* 39, 5241–5255. <https://doi.org/10.1002/joc.6136>.
- Xin, J., Sun, X., Liu, L., Li, H., Liu, X., Li, X., Cheng, L., Xu, Z., 2021. Quantifying the contribution of climate and underlying surface changes to alpine runoff alterations associated with glacier melting. *Hydrol. Process.* 35, 1–26. <https://doi.org/10.1002/hyp.14069>.
- Xu, D., Lin, Y., 2021. Impacts of irrigation and vegetation growth on summer rainfall in the taklimakan desert. *Adv. Atmos. Sci.* 38, 1863–1872. <https://doi.org/10.1007/s00376-021-1042-x>.
- Xu, X., Yang, D., Yang, H., Lei, H., 2014. Attribution analysis based on the Budyko hypothesis for detecting the dominant cause of runoff decline in Haihe basin. *J. Hydrol.* 510, 530–540. <https://doi.org/10.1016/j.jhydrol.2013.12.052>.
- Yan, H., Huang, J., He, Y., Liu, Y., Wang, T., Li, J., 2020. Atmospheric water vapor budget and its long-term trend over the Tibetan Plateau. *J. Geophys. Res. Atmos.* 125, 1–17. <https://doi.org/10.1029/2020JD033297>.
- Yang, K., He, J., Tang, W., Qin, J., Cheng, C.C.K., 2010. On downward shortwave and longwave radiations over high altitude regions: observation and modeling in the Tibetan Plateau. *Agric. Meteorol.* 150, 38–46. <https://doi.org/10.1016/j.agrformet.2009.08.004>.
- Yang, Z., Qian, Y., Liu, Y., Berg, L.K., Hu, H., Dominguez, F., Yang, B., Feng, Z., Gustafson, W.I., Huang, M., Tang, Q., 2019. Irrigation impact on water and energy cycle during dry years over the United States using convection-permitting WRF and a dynamical recycling model. *J. Geophys. Res. Atmos.* 124, 11220–11241. <https://doi.org/10.1029/2019JD030524>.
- Yang, P., Xia, J., Zhang, Y., Hong, S., 2017. Temporal and spatial variations of precipitation in Northwest China during 1960–2013. *Atmos. Res.* 183, 283–295. <https://doi.org/10.1016/j.atmosres.2016.09.014>.
- Yao, J., Chen, Y., Guan, X., Zhao, Y., Chen, J., Mao, W., 2022. Recent climate and hydrological changes in a mountain-basin system in Xinjiang, China. *Earth-Sci. Res.* 226, 103957 <https://doi.org/10.1016/j.earscirev.2022.103957>.
- Yao, J., Chen, Y., Zhao, Y., Guan, X., Mao, W., Yang, L., 2020. Climatic and associated atmospheric water cycle changes over the Xinjiang, China. *J. Hydrol.* 585, 124823 <https://doi.org/10.1016/j.jhydrol.2020.124823>.
- Yu, Y., Notaro, M., Wang, F., Mao, J., Shi, X., Wei, Y., 2017. Observed positive vegetation-rainfall feedbacks in the Sahel dominated by a moisture recycling mechanism. *Nat. Commun.* 8, 1–9. <https://doi.org/10.1038/s41467-017-02021-1>.
- Yu, M., Wang, G., Pal, J.S., 2016. Effects of vegetation feedback on future climate change over West Africa. *Clim. Dyn.* 46, 3669–3688. <https://doi.org/10.1007/s00382-015-2795-7>.
- Zemp, D.C., Schleussner, C.F., Barbosa, H.M.J., Hirota, M., Montade, V., Sampaio, G., Staal, A., Wang-Erlandsson, L., Rammig, A., 2017. Self-amplified Amazon forest loss due to vegetation-atmosphere feedbacks. *Nat. Commun.* 8 <https://doi.org/10.1038/ncomms14681>.
- Zeng, Y., Milly, P.C.D., Shevliakova, E., Malyshev, S., van Huijgevoort, M.H.J., Dunne, K.A., 2022. Possible anthropogenic enhancement of precipitation in the sahel-sudan savanna by remote agricultural irrigation. *Geophys. Res. Lett.* 49, 1–10. <https://doi.org/10.1029/2021GL096972>.
- Zeng, Z., Piao, S., Li, L.Z.X., Wang, T., Ciais, P., Lian, X., Yang, Y., Mao, J., Shi, X., Myneni, R.B., 2018. Impact of Earth greening on the terrestrial water cycle. *J. Clim.* 31, 2633–2650. <https://doi.org/10.1175/JCLI-D-17-0236.1>.
- Zhang, F., Huang, T., Man, W., Hu, H., Long, Y., Li, Z., Pang, Z., 2021. Contribution of recycled moisture to precipitation: a modified d-excess-based model. *Geophys. Res. Lett.* 48, 1–12. <https://doi.org/10.1029/2021GL095909>.
- Zhang, C., Tang, Q., Chen, D., Li, L., Liu, X., Cui, H., 2017. Tracing changes in atmospheric moisture supply to the drying Southwest China. *Atmos. Chem. Phys.* 17, 10383–10393. <https://doi.org/10.5194/acp-17-10383-2017>.
- Zhao, L., Liu, X., Wang, N., Kong, Y., He, Z., Liu, Q., Wang, L., 2019. Contribution of recycled moisture to local precipitation in the inland Heihe River Basin. *Agric. For. Meteorol.* 271, 316–335. <https://doi.org/10.1016/j.agrformet.2019.03.014>.